Incidence of Phage Capsid Organization on the Resistance to High Energy Proton Beams

Laura Maria De Plano [1,*], Letteria Silipigni [2], Lorenzo Torrisi [2], Alfio Torrisi [3], Mariapompea Cutroneo [4,*], Vladimir Havranek [4], Anna Mackova [4,5], Vincenzo Zammuto [1], Concetta Gugliandolo [1], Maria Giovanna Rizzo [1], Salvatore P. P. Guglielmino [1] and Domenico Franco [1]

[1] Department of Chemical, Biological, Pharmaceutical and Environmental Sciences, University of Messina, 98166 Messina, Italy; vzammuto@unime.it (V.Z.); cgugliandolo@unime.it (C.G.); mgrizzo@unime.it (M.G.R.); sguglielm@unime.it (S.P.P.G.); dfranco@unime.it (D.F.)

[2] Department of Mathematical and Computational Sciences, Physical Sciences and Earth Sciences, University of Messina, 98166 Messina, Italy; lsilipigni@unime.it (L.S.); ltorrisi@unime.it (L.T.)

[3] Department of Mathematics and Physics "E. De Giorgi"—CEDAD (CEnter of Applied Physics, DAting and Diagnostics), University of Salento, 73100 Lecce, Italy; alfio.torrisi@unisalento.it

[4] Department of Neutron Physics, Institute of Nuclear Physics, v.v.i., Husinec-Řež 130, 25068 Řež, Czech Republic; havranek@ujf.cas.cz (V.H.); mackova@ujf.cas.cz (A.M.)

[5] Department of Physics, Faculty of Science, J. E. Purkyne University, Pasteurova 3544/1, 400 96 Usti nad Labem, Czech Republic

* Correspondence: ldeplano@unime.it (L.M.D.P.); cutroneo@ujf.cas.cz (M.C.)

Abstract: The helical geometry of virus capsid allows simple self-assembly of identical protein subunits with a low request of free energy and a similar spiral path to virus nucleic acid. Consequently, small variations in protein subunits can affect the stability of the entire phage particle. Previously, we observed that rearrangement in the capsid structure of M13 engineered phages affected the resistance to UV-C exposure, while that to H_2O_2 was mainly ascribable to the amino acids' sequence of the foreign peptide. Based on these findings, in this work, the resistance to accelerated proton beam exposure (5.0 MeV energy) of the same phage clones was determined at different absorbed doses and dose rates. Then, the number of viral particles able to infect and replicate in the natural host, *Escherichia coli* F+, was evaluated. By comparing the results with the M13 wild-type vector (pC89), we observed that 12III1 phage clones, with the foreign peptide containing amino acids favorable to carbonylation, exhibited the highest reduction in phage titer associated with a radiation damage (RD) of $35 \times 10^{-3}/Gy$ at 50 dose Gy. On the other hand, P9b phage clones, containing amino acids unfavorable to carbonylation, showed the lowest reduction with an RD of $4.83 \times 10^{-3}/Gy$ at 500 dose Gy. These findings could improve the understanding of the molecular mechanisms underlying the radiation resistance of viruses

Keywords: M13 bacteriophages; engineered phage clones; proton beam radiation; resistance to particles radiation

1. Introduction

The last decades have been characterized by viral epidemics that led to the coronavirus pandemic in 2020 and 2021 [1,2]. This places as the main objective of numerous research groups the development of protocols and predictive studies to understand evolutionary ecology and the emergence of new virus variants [3,4]. On the other hand, both epidemiological and patient-based approaches are often late in avoiding pandemic events due to the ability of viruses to quickly gain new infective features during pandemic advancement [5].

Molecular mechanisms, which can occur in natural mutations, determine both the emergence and the spread of new viral variants. In this context, the increase in knowledge could help the protocols of disinfection or virus inactivation (for vaccine development),

that are often slowed down due to the difficulties related to cultivation techniques and/or high contagiousness.

Bacteriophages (or shortly phages) represent models extremely useful for understanding the molecular mechanisms involved in the stability of viral capsids and the resistance to different stresses. Similar to mammalian virus, phage resistance to environmental stresses is closely related to the protein composition of the external structure, named capsid, which encloses and protects the viral nucleic acid. In addition, it is known that the dynamic rearrangements or disassembly of capsid can affect the nucleic acid release in the host, consequently determining the success or failure of the infectious process [6]. The most common capsid geometries are icosahedral or helical symmetry. In the first case, the nucleic acid of a virus is packaged completely within a geometric shape with 20 sides with morphological units (capsomeres) arising from the interaction of proteins within the repeated structural units [7]. Differently to this, the helical array winds around the nucleic acid, following a similar spiral path, and can require only one nucleocapsid protein. Since a single alteration in the capsid proteins' subunits affect the stability of the entire phage particle, the use of helical phages, engineered to express specific changes on known portions of their protein subunits, could help to identify the cause–effect relationships between specific mutations and new structural rearrangements in the capsid.

M13 phage has been widely used in several applications due to its nontoxic, self-assembling and specific binding properties. The small DNA and use as a vector for constructing phage libraries displaying billions of random peptides on the phage surface, made this phage (together with the other filamentous phages fd and f1) a model system in molecular biology and a versatile tool in genetic engineering and biotechnology [8]. The capsid of M13 phage, characterized by a helical symmetry structure, is mainly constituted by the major coat protein pVIII, which is responsible for the integrity of the phage. Vector systems-based phage libraries 88 or 8 + 8 result in a hybrid structure with a mixture of recombinant and wild-type pVIII molecules on the phage capsid [9]. The use of these random phage libraries is being increased in many biotechnological applications, such as marker discovery in vitro or in vivo [10,11], surface functionalization for biosensors [12–14], as specific scaffolds for tissue-regeneration [15], immunization [16], drug targeting [17,18] and hybrid materials [19–22]. However, since M13 capsid is approximately composed by 2700 copies of the major coat protein pVIII, the virion particles could show a remarkable degree of conformational instability and/or metastability when engineered on pVIII protein [23]. The capsid structure has been suggested to be responsible for the great resistance of M13 to various physical and chemical stresses [20,24,25]. Moreover, we recently reported that the addition of foreign peptides in M13-engineered phages modified the spatial distribution of surface charges and the stretching of the entire capsid, affecting their resistance against UV-C exposure and H_2O_2 treatment [26,27].

Ionizing radiation can damage biological components though the direct deposition of radiation energy into biomolecules and also indirectly by generating reactive oxygen species (ROS). Hydrogen peroxide (H_2O_2) and hydroxyl radicals (HO•) are major oxidizing species produced by the radiolysis of water, and superoxide ions ($O2•−$) are formed in the presence of dissolved oxygen [28]. Generally, the cytotoxic and mutagenic effects induced by ionizing radiation are thought to be the result of DNA damage caused during the course of irradiation, which includes single-strand breaks (SSB), double-strand breaks (DSB), base modification and sugar modification [29]. The amounts of radiation damage caused by given doses of ionizing radiation for different microorganisms or biomolecules are very similar, although the range of ionizing radiation resistance levels is large [30].

In order to increase our knowledge on the viral resistance to radiations, in this work, the incidence of phage capsid organization of M13-engineered phages on the resistance to high energy proton beams was evaluated. Specifically, the viability of pC89 (M13 wild-type vector) and two engineered phage clones, expressing 9 or 12 additional amino acids in the N-terminal end of pVIII capsid protein, was determined at different absorbed doses and dose rates.

2. Materials and Methods

2.1. Bacteriophages

Engineered phages were obtained from M13 phage libraries, constructed in the vector pC89 [31], by cloning a random DNA insert between the third and fifth codon of the mature pVIII-encoding segments of gene VIII [32]. Specifically, the P9b phage clone was selected from a 9-mer phage library, and it displays the 9 amino acid sequence, QRKLAAKLT, which is fused to the major coat protein (pVIII) and is able to specifically recognize *Pseudomonas aeruginosa* [33]. In addition, 12III1 phage clone was obtained by screening of 12-mer phage library against anti-Caf1 monoclonal antibody and IgGs from AD-patients, in alternate biopanning cycles, named "double binding" selection. 12III1 display the 12 amino acid sequence, RWPPHFEWHFDD, able to detect IgG levels correlated with Alzheimer disease [34]. All radiation tests were carried out using the insert-less pC89 vector as wild-type virus variant.

2.2. Phage Propagation

pC89 and engineered phage clones (Amp+) were propagated in the bacterial host *Escherichia coli* strain TG1 (Kan-, Amp-, lacZ-), according to Kay et al. [35] with some modifications for our conditions. For each phage, an overnight culture of *E. coli* was reinoculated in fresh Luria–Bertani medium (LB) at 250 rpm on a rotary shaker for about 3 h at 37 °C, until reaching an optical density at 600 nm (OD_{600}) equal to 0.7. After incubation period, *E. coli* culture was infected with each phage and incubated at 37 °C, in static condition for 15 min and at 250 rpm on a rotary shaker for 20 min. After incubation, infected *E. coli* was plated onto LA (Luria–Bertani added with agar 20 g/L) plates containing ampicillin (50 µg/mL). Plates were incubated overnight at 37 °C in static condition. From each plate, one colony of *E. coli* containing phage, was inoculated into 10 mL of LB medium containing ampicillin (50 µg/mL) and incubated at 250 rpm on a rotary shaker at 37 °C for 3–4 h, until OD_{600} equal to 0.2 was reached. After incubation, the culture was added with isopropylthio-β-galactoside (IPTG, 40 µg/mL) and helper phage M13K07 (Kan+) (10^9 transduction units per milliliter, TU/mL), incubated at 37 °C, in static condition for 15 min and at 250 rpm on a rotary shaker for 20 min. After incubation, culture was centrifugated at $8000 \times g$ for 20 min, supernatant removed, replaced with LB medium containing ampicillin (50 µg/mL) and kanamycin (10 µg/mL), and incubated overnight with shaking at 37 °C.

2.3. Phage Collection

Phages were collected from the bacterial host culture by means of several centrifugation steps in PEG/NaCl solution, containing 200 g PEG-8000 (polyethylene glycol; Sigma-Aldrich, Milan, Italy) and 150 g NaCl (Sigma-Aldrich, Milan, Italy) per liter. Specifically, culture was centrifuged at $8000 \times g$ for 20 min at 25 °C, supernatant recovered and mixed with 25% (*v/v*) of PEG/NaCl solution. The mixture was cooled in ice for 4 h and precipitated by centrifugation at $15,000 \times g$ for 45 min at 4 °C. The pellet was recovered, resuspended in 10% (*v/v*) of Tris-buffered saline (TBS, 7.88 g/L of Tris hydrochloride and 8.77 g/L of NaCl in deionized water), mixed again with 25% (*v/v*) of PEG/NaCl, cooled in ice for 4 h, and the solution was centrifuged as above. The pellet, containing phage particles, was suspended in 10% (*v/v*) of TBS, filtered through 0.22 µm pore size membrane (Millipore) and stored at 4 °C.

2.4. Proton Irradiations

In total, 200 µL suspensions of each phage stocks in Tris-buffered saline (TBS; 7.88 g/L of Tris hydrochloride and 8.77 g/L NaCl in deionized water) were exposed at room temperature to proton beams. To this, 200 µL solution was capsuled in a small polyethylene (PE) holder with a wall thickness of 25 mm. The holder shape is cylindrical with 10 mm radius and 637 µm height, corresponding to a volume of 200 mm³. Outside of the chamber is located a PIN diode for the measure of the low current rate of particle/s. It was measured 10^5 particle/s and a sensitivity of current of 1 pA corresponding to a rate of

100 pulse/s. The attested dose values were further justified by the evaluations obtained using gaf-chromics [36] placed on the front side of the holder hosting the phages.

All irradiations were carried out in the Nuclear Physics Institute of Rez (Czech Republic) using the proton beam extracted in air at the maximum energy of 5 MeV [37]. Protons were accelerated by a Tandetron accelerator and led [38] to a holder placed inside the vacuum chamber containing a YAG Cs scintillator to set the beam size and focus, Cu mesh to probe the resolution and a small faraday cup to measure the current of proton beam. Finally, protons were extracted from high vacuum to air through 200 nm Si_3N_4 film, of which density is 3.17 g/cm^3. The proton energy loss in this film is DE_1 = 4 keV. Protons cross 2 mm air thickness before hitting the PE holder, losing an energy of DE_2 = 16.4 keV. Crossing the PE wall thickness protons lose another DE_3 = 261.5 keV, to reach the solution containing the phages, with a kinetic energy of 4718 keV.

To fulfil the demands of uniform irradiation of the solution, the proton irradiation was accomplished using a proton microbeam with a size of 500 mm $\times$ 530 mm, which was swept on an area of 24 mm $\times$ 20.1 mm. The scan velocity is 1.985 mm/s, the step resolution is 0.3 mm and the total number of horizontal sweep lines is 67. The irradiated surface was S = 4.8 cm^2 and the used proton fluence F_i ranges between 2.3 $\times$ 10^7 H$^+$/sA and 2.3 $\times$ 10^8 H$^+$/sA. The solution was irradiated by high proton energy at 4718 keV and low energy around 100 keV.

2.5. Dose Absorbed (Da) and Dose Rate

The dose absorbed by the biological solution containing the phages, D_a, in terms of energy deposited for mass unit (Gy), was calculated taking into consideration the above-described proton irradiation conditions as follows [39]

$$D_a \ (\text{Gy}) = F_i \times S_t \times \frac{1}{r} \tag{1}$$

where F_i is the ion fluence calculated in ions/cm^2 units, S_t the total stopping power given in keV/μm and r the mass density in g/cm^3 of the irradiated solution. Irradiations were performed using doses from 5 up to 500 Gy and dose rates, obtained dividing for the irradiation time, from 0.00615 up to 0.615 Gy/s. Doses and dose rates have uncertainties lower than 5%.

2.6. Phage Titration (TU/mL)

After proton beam exposure, tenfold serial dilutions of each phage were prepared. Then, 10 μL from each dilution sample were dispensed into sterile micro-centrifuge tubes containing 90 μL of *E. coli* TG1 culture at OD_{600} equal to 0.7. Tubes were incubated at 37 °C in static condition for 15 min and at 250 rpm on a rotary shaker for 20 min. After incubation, 100 μL of each phage/*E. coli* TG1 suspension were dispensed into LA plates containing ampicillin (50 μg/mL) and incubated at 37 °C overnight. Plates, containing between 30–300 colonies, were counted to derive the number of active viral particles able to infect the host cell and express the transgene. Thus, the active particles were determined by transducing units per milliliter (TU/mL), according to the following Equation (2)

$$\frac{\text{TU}}{\text{mL}} = \frac{(\text{number of colonies})}{\text{volume (0.1 mL)} \times \text{dilution factor}} \tag{2}$$

All assays were performed in quintuplicate.

2.7. Radiation Damage (RD)

The radiation damage (RD) was defined as the effect of the high energy protons beam on phage ability to infect its host and express the transgene. It represents the logarithmic

inactivation of phage titer per absorbed dose in Gy and can be derived from the following Equation (3)

$$\text{RD} = \frac{\log_{10} \text{Ns(i)} - \log_{10} \text{Ns(r)}}{\text{Dose (Gy)}} \tag{3}$$

where Ns(i) and Ns(r) are M13 particles not irradiated and after irradiation, respectively. In order to exclude any changes due to overall long-term stability of phages, the not irradiated samples followed the same travel and storage of irradiated samples. The significant differences in the RD values were determined by analysis of variance (ANOVA) using adjusted *p*-values at 0.01 and 99% for family-wise significance and confidence level, respectively.

3. Results and Discussion

In order to have a proper proton–solution interaction, each phage solution (200 μL) in small polyethylene (PE) holders was treated according to the experimental set-up described in Figure 1.
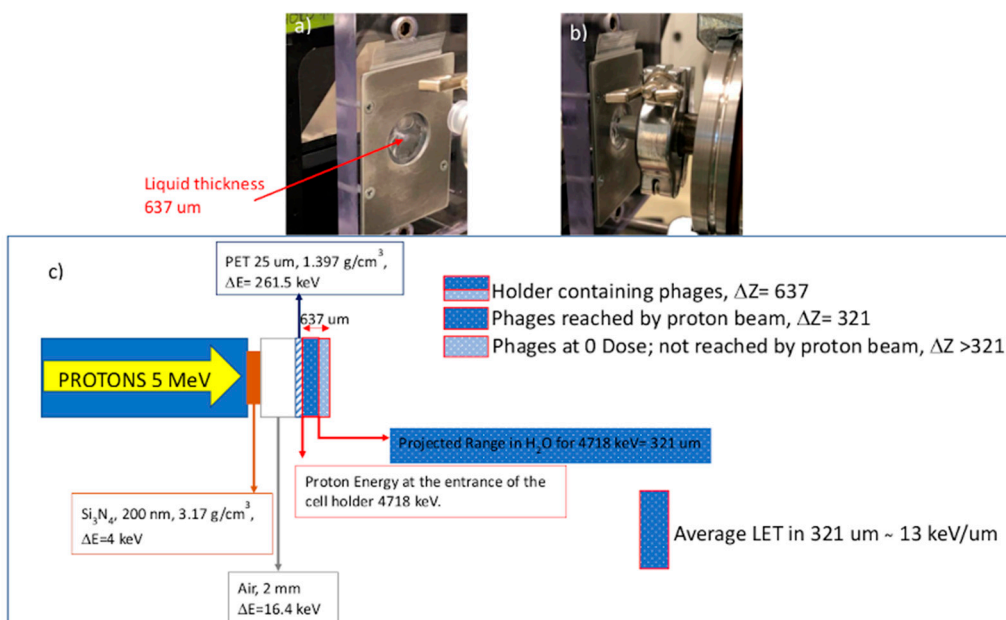

Figure 1. Holder made of PE, containing the phage solution (**a**), detail of the set-up adopted for the proper proton–solution interaction (**b**) and scheme of the proton energy loss in the different materials before hitting the phage solution (**c**).

Since the proton path is affected by the chemical–physical features of the holder, preliminary tests with different materials were carried out to evaluate the proton energy loss before hitting the viral solution (data not shown). In our experimental conditions, the projected ion range in the solution was 321 μm, thus, only 50% of the solution thickness was irradiated. To this, the solution holder was subjected to fast oscillations, which, producing liquid mixing, permitted irradiation of the entire solution during the 800 s irradiation time. Experiments were carried out in the regimes of electron energy loss and nuclear energy loss, respectively, because each phage solution was irradiated by high proton energy (4718 keV) and low energy (around 100 keV). In the first case, ionizations were mainly produced along the proton path, while in the second case, scissions, atomic collisions and the breaking of chemical bonds occurred.

Figure 2a reports the SRIM simulations [40] of the proton trajectories inside the liquid solution, assumed as "water-like", while Figure 2b shows the stopping power trend versus the solution depth, indicating the different stopping at the target surface (electronic) and at the Bragg peak (maximal stopping at the end of ion path). From the latter, it can be deduced that the minimum stopping power is 8 keV/μm, while the maximum, at the Bragg

peak, is 40 keV/μm. By considering the shape of the proton stopping power vs. depth, the average weight of its value is about 13 keV/μm, which is considered to be the average linear energy transfer (LET) of the proton radiation in the irradiated solution.
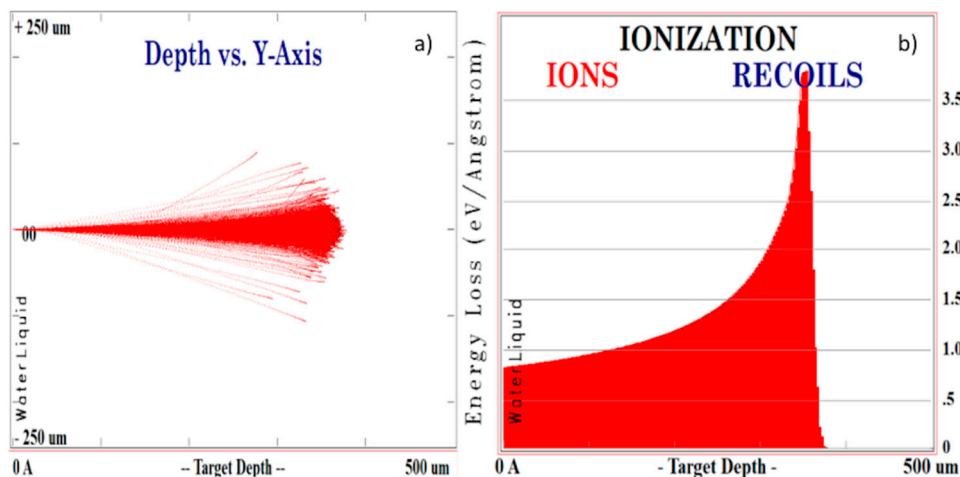

Figure 2. Proton penetration in the water solution (**a**) and stopping power of the protons along the solution depth (**b**).

It is known that the proteins are prominently targeted by radiations, which induce oxidation or reduction in the functional groups exposed on the chains [41,42]. Consequently, the resistance to radiation stress could depend on the maintenance of the capsid structure, especially against indirect damage, due to radiolytic OH− and H+ products resulting from the water radiolysis. In more complex structures, such as that of bacteriophage M13, the pVIII proteins form a tube-like structure around DNA. Specifically, each coat protein is oriented with the N-terminus, located at the outside, and the C terminus at the inside to interact with the DNA [43]. Moreover, the hydrophobic domain, located in the central part, interlocks the coat protein with those neighboring [44]. Consequently, small variations in protein subunits can affect the stability of the entire phage particle.

To this purpose, two phage clones, engineered to display in pVIII capsid protein foreign peptides of 9 (P9b) and 12 amino acids (12III1), were evaluated for their ability to maintain infectious and replicative properties after exposure to accelerated proton beams at 5.0 MeV energy, 3.8–38 pA beam current, 50–500 Gy absorbed dose and 0.0615–0.615 Gy/s dose rate (Table 1).

Table 1. Used dose and dose rates for phage solution proton irradiation.

Dose (Gy)				
50	125	250	375	500
Dose Rate (Gy/s)				
0.0615	0.155	0.309	0.463	0.615

Although the absorbed doses were high, their administration to the phage solution was given slowly (Table 1), thus, the dose rate was low, giving time to the molecular structures to reorganize and to the biological structures to partially repair the damage suffered.

Phage clones were chosen on the basis of the amino acid sequence of the foreign peptide displayed on the engineered pVIII protein. Specifically, 12III1 foreign peptide contains amino acids with aromatic (4), negatively (3) and positively (3) R-groups that are highly responsive to oxidation products from water radiolysis, such as with OH⁻ addition to the aromatic ring or carbonylation reaction. Moreover, oxidation by reactive oxygen species (ROS) could also include the production of carbonyl groups on the amino acid side

chain of proline residues. On the other hand, in P9b, the presence of aliphatic amino acids, namely leucine (2) and alanine (2), in foreign peptide should maintain the capsid's integrity and, therefore, the phage clone is less susceptible to oxidative stress. All experiments were carried out using M13 wild-type vector without the peptide insert (pC89) as control. Results on the viability of pC89, P9b and 12III1 phages after exposure to proton beam radiation are reported in Table 2.

Table 2. Active virus particles of pC89, P9b and 12III1, expressed as transducing unit per milliliter of infected *E. coli* (TU/mL), at different dose (Gy) of 5 MeV proton irradiation. In brackets are survival percentages compared to exposed phages. Each value has been derived as averages from 5 replicates with standard deviations.

Phage Clone	Exposed	Dose (Gy)				
		50 Gy	125 Gy	250 Gy	375 Gy	500 Gy
pC89	$(3.0 \pm 0.14) \times 10^{10}$ (100%)	$(2.1 \pm 0.3) \times 10^{10}$ (70%)	$(7.1 \pm 0.27) \times 10^{8}$ (2.37%)	$(3.0 \pm 0.41) \times 10^{8}$ (1%)	$(1.1 \pm 0.8) \times 10^{8}$ (0.37%)	$(1.0 \pm 0.5) \times 10^{7}$ (0.033%)
P9b (QRKLAAKLT)	$(2.6 \pm 0.21) \times 10^{10}$ (100%)	$(2.0 \pm 0.25) \times 10^{10}$ (77%)	$(1.1 \pm 0.17) \times 10^{10}$ (42.3%)	$(5.0 \pm 0.34) \times 10^{9}$ (19.2%)	$(2.4 \pm 0.45) \times 10^{9}$ (9.2%)	$(1.0 \pm 0.49) \times 10^{8}$ (0.38%)
12III1 (RWPPHFEWHFDD)	$(3.0 \pm 0.38) \times 10^{10}$ (100%)	$(5.1 \pm 0.23) \times 10^{8}$ (17%)	$(3.0 \pm 0.39) \times 10^{7}$ (0.1%)	$(1.9 \pm 0.5) \times 10^{7}$ (0.063%)	$(4.7 \pm 0.48) \times 10^{6}$ (0.0157%)	$(1.4 \pm 0.51) \times 10^{4}$ (0.00047×10%)

Data show that at the maximum absorbed proton dose (500 Gy) the most resistant phage was P9b (0.38% of survival), while the least resistant was 12III1 (0.00047%). Finally, an intermediate level of resistance was exhibited by the pC89 (0.033%). This trend of susceptibility was observed at each dose Gy, and P9b was always the most resistant phage, while the least was 12III1 (Figure 3a).
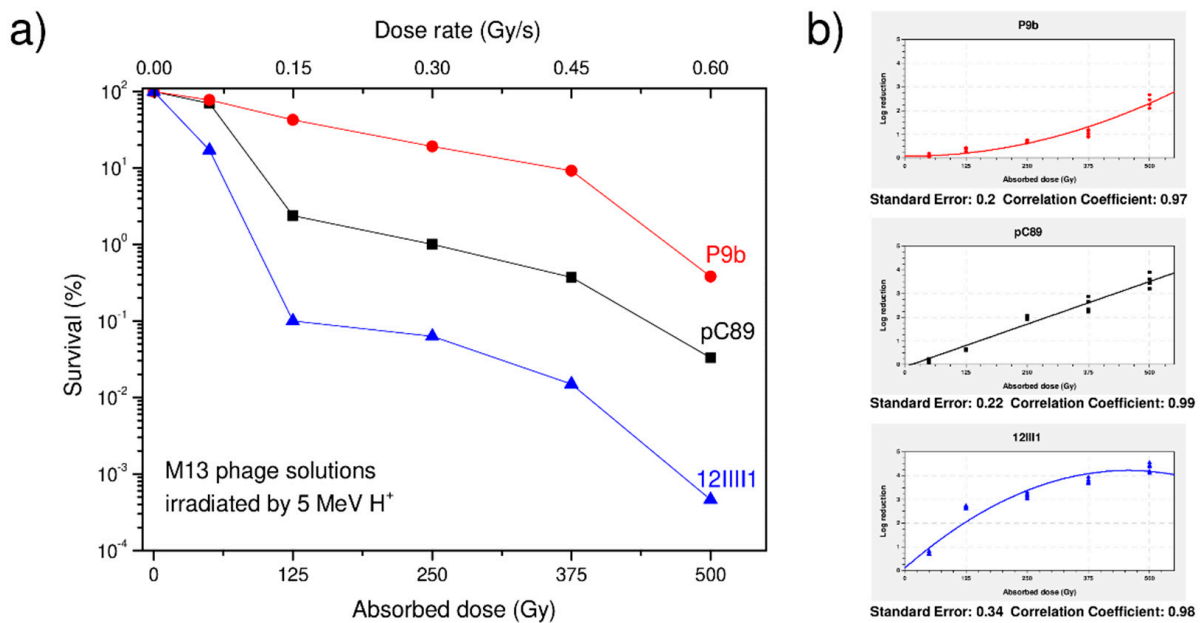

Figure 3. Susceptibility trend of pC89, 12III1 and P9b to proton beam radiation in terms of survival percentage (**a**) and logarithmic viability reduction (**b**).

Since the tested phages have the same DNA, with the exception of the small insert displaying the foreign peptide on the major coat proteins, it is very likely that the difference in susceptibility is due to the presence/absence and amino acid composition of the foreign peptide. The latter does not affect the replication of the phage but determines its susceptibility in the presence of radiation stress. Moreover, since the experimental plan for each phage was carried out in about 800 s continuum irradiation time, the same trend was

also found in terms of the dose rate in the range 0.0615–0.615 Gy/s, as specified in Table 1. Interestingly, when evaluated in terms of logarithmic reduction as a function of the proton absorbed dose, the tested phages showed different trends (Figure 3b). In fact, pC89 showed a linear trend of the logarithmic reduction with increasing proton absorbed dose, whereas the two engineered phages exhibited a quadratic trend with a saturation phase of the log reduction at the maximum tested dose for 12III1 and a lag phase at the lowest dose for P9b. These findings indicate that the action of resistance to the proton radiation was maintained in P9b up to the dose of 375 Gy, beyond which the phage began to lose vitality; on the other hand, 12III1 showed a loss of vitality at all doses, even higher than that of pC89, revealing an almost absence of resistance already at the first exposure dose of proton radiation. It is known that coat proteins have a critical role both during the infectious process of entry and assembly of the new virion [45]. Consequently, the coat protein structure and its dynamicity during the virus reproduction cycle must be maintained. Our findings show that P9b did not suffer damage (including any lethal mutations) that would interfere with its correct infectious cycle.

Based on Equation (3), we deduced the radiation damage (RD) for the proton beam by the logarithmic values of the phage survival. These findings are supported by the RD ranges for each phage clone between the minimum (50 Gy) and high levels (500 Gy), which are reported in Table 3.

Table 3. Radiation damage (RD, $\times 10^{-3}$ Gy^{-1}) for each phage at different doses (Gy) of 5 MeV proton irradiation.

Phage Clone	50 Gy	125 Gy	250 Gy	375 Gy	500 Gy
pC89	3.1	13	8.0	6.5	6.95
P9b (QRKLAAKLT)	2.28	2.99	2.86	2.75	4.83
12III1 (RWPPHFEWHFDD)	35.4	24.0	12.8	10.1	10.7

RD was very high in the case of 12III1, arriving at values of the orders of 35×10^{-3}/Gy at 50 dose Gy, and decreasing with increasing exposure doses. These findings agree with those from Figure 3 and confirm the almost total absence of resistance of 12III1 to proton radiation, as evidenced by higher RD values at lower exposure doses. On the other hand, P9b showed a low and constant RD value, with a slight increase at the highest dose tested (500 Gy), revealing high resistance to all doses tested. Finally, an intermediate trend was observed for pC89, which showed the maximum RD value at the dose of 125 Gy.

The RD trend of each phage as a function of the absorbed proton dose and the dose rate is shown in Figure 4.
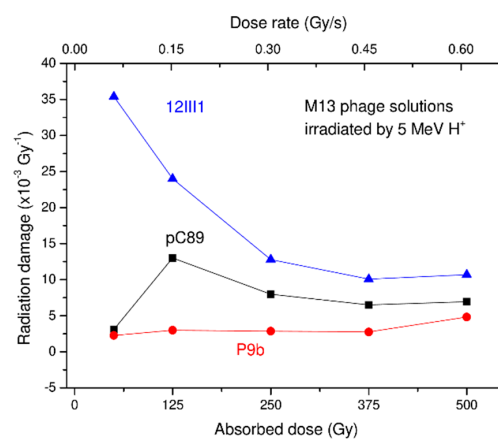

Figure 4. Radiation damage (RD) for each phage as a function of absorbed proton dose and the dose rate.

Results indicated that, while 12III1 and pC89 reached the maximum RD at 35.4 and 13 dose Gy, respectively, P9b had still not reached the maximum RD value. Moreover, RD values from all phages tended to become closer at the maximum total dose. Since RD represents the logarithmic inactivation of phage titer per absorbed dose in Gy, the more susceptible phages will have high values at low doses, as in the case of 12III1 and pC89, and a negative correlation as the dose Gy is increased, due to the fact that most of the phage titer has already been lost at the first doses. Along with those described above, these results indicated that the resistance to irradiations was probably dependent on the maintenance of the capsid structural integrity. The different behaviours of the three phages exposed to the proton beam could be correlated with a different degree of interaction between pVIII–pVIII proteins, due to the peptides exposed in their N-terminus. In a previous work, we observed that the presence of a foreign amino acid sequence on the capsid protein pVIII of P9b and 12III1 phage clones generated an increase in H-bonds and steric interactions in capsid proteins, resulting in the increased resistance to UV-C radiation damage [26].

The comparison of the susceptibility to the proton beam and UV-C of the three phages is reported in Figure 5.
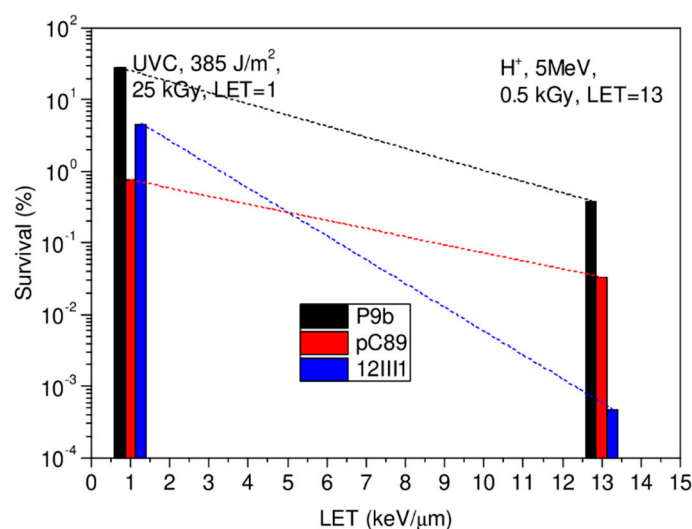

Figure 5. Susceptibility comparison of pC89, P9b and 12III1 phages to proton beam and UV-C.

It is well known that ionizing radiations induce damage proportionally to the radiation LET and the plot of the damage vs. LET represents an important aspect for many experts, especially in the field of Physics, Chemistry, Radiology, Biology and Medicine. It is expected that phage survival decreases with the LET value of the used ionizing radiation, as indicated by the dashed lines in Figure 5. Therefore, a lower dose for protons and a higher dose for photons was needed for the inactivation of the virus.

Although the UV–protons comparison (Figure 5) was performed at comparable doses, the data indicated a noticeable change in the susceptibility to UV-C and proton beam exposure of 12III1, compared to wild-type pC89. The survival ratio P9b/pC89 was 37.6 for UV and 11.5 for protons, while the survival ratio 12III1/pC89 was 6.13 for UV and 0.014 for protons. Thus, proton beams induced major damage compared with UV photons in all the investigated phages, as expected by the major radiation LET. Concordantly, the survival percentage was reduced from a factor 23 up to a factor 9800 using protons. A possible explanation could be derived from the different nature of the two radiations, in that, when phages are exposed to UV-C radiation, the damage could be predominantly ascribed to the direct effects of absorbed radiation by nucleic acids [46]. The formation of dimers (cyclobutane pyrimidine and pyrimidine) and photoproducts (pyrimidine) has been reported to increase in proportion to the UV-C dose, modifying the DNA structure. On the other hand, when the same phage clones are exposed to the proton beam, they could also be subjected to indirect damage due to OH- and H+ products resulting from the

water radiolysis [47]. Differently to P9b, 12III1 foreign peptide, composed by aromatic and other amino acids favorable to carbonylation, could be subjected to a high degree of oxidative modifications and, consequently, a fragmentation of the protein backbone. These findings are in accordance with our previous results, obtained by treating the same phages with H_2O_2 [26]. In fact, in these experimental conditions, only P9b showed an increased resistance to induced stress, while no significant difference was recorded between 12III1 and pC89.

4. Conclusions

In order to study the incidence of capsid organization on the resistance to high energy proton beams, M13 wild-type vector and two engineered phage clones, expressing 9 or 12 additional amino acids in the N-terminal end of pVIII capsid proteins, were evaluated.

Results indicated that the radiation damages, induced by different ion doses and dose rates, depended on the amount of ionizing energy transferred to the phages. On the other hand, although the phage viability decreased exponentially with the ion dose, the resistance of each phage to the same dose depended on the amino acid composition of their capsid proteins.

Although we cannot actually distinguish between the electronic and the nuclear damage, the energy released from the radiation could destabilize the entire capsid structure and, therefore, make the nucleic acid more exposed to the radiolitic effects. Our findings showed that 12III1, containing almost exclusively amino acids favorable to carbonylation in foreign peptide, resulted in being the most susceptible to radiation, while P9b, exposing amino acids not favorable to carbonylation, was the most resistant. These findings suggest that modification in protein subunits could have compromised or further stabilized the entire virion, although further experiments will be performed to separate electronic from nuclear defects in the investigated phage structures. The study of the structure–function and self-assembly of new protein subunits in the capsid, together with the response of the latter in physical stresses, such as ionizing radiation, is needed to understand the molecular mechanisms that underlie the onset and spread of virus variants and, in turn, to allow faster and more effective approaches in the fight against viral disease.

References

1. Roychoudhury, S.; Das, A.; Sengupta, P.; Dutta, S.; Roychoudhury, S.; Choudhury, A.P.; Ahmed, A.B.F.; Bhattacharjee, S.; Slama, P. Viral Pandemics of the Last Four Decades: Pathophysiology, Health Impacts and Perspectives. *Int. J. Environ. Res. Public Health* **2020**, *17*, 9411. [CrossRef]
2. Zhou, P.; Yang, X.L.; Wang, X.G.; Hu, B.; Zhang, L.; Zhang, W.; Si, H.R.; Zhu, Y.; Li, B.; Huang, C.L.; et al. A pneumonia outbreak associated with a new coronavirus of probable bat origin. *Nature* **2020**, *579*, 270–273. [CrossRef]
3. Dennehy, J.J. Evolutionary ecology of virus emergence. *Ann. N. Y. Acad. Sci.* **2017**, *1389*, 124–146. [CrossRef]
4. Snedden, C.E.; Makanani, S.K.; Schwartz, S.T.; Gamble, A.; Blakey, R.V.; Borremans, B.; Helman, S.K.; Espericueta, L.; Valencia, A.; Endo, A.; et al. SARS-CoV-2: Cross-scale Insights from Ecology and Evolution. *Trends Microbiol.* **2021**, *29*, 593–605. [CrossRef]

5. Excler, J.-L.; Saville, M.; Berkley, S.; Kim, J.H. Vaccine development for emerging infectious diseases. *Nat. Med.* **2021**, *27*, 591–600. [CrossRef]
6. Perlmutter, J.D.; Hagan, M.F. Mechanisms of virus assembly. *Annu. Rev. Phys. Chem.* **2015**, *66*, 217–239. [CrossRef]
7. Prasad, B.V.V.; Schmid, M.F. Principles of virus structural organization. In *Viral Molecular Machines*; Rossmann, M.G., Rao, V.B., Eds.; Springer: Boston, MA, USA, 2012; pp. 17–47.
8. Petrenko, V.A. Landscape Phage: Evolution from Phage Display to Nanobiotechnology. *Viruses* **2018**, *10*, 311. [CrossRef] [PubMed]
9. Smith, G.P.; Petrenko, V.A. Phage display. *Chem. Rev.* **1997**, *97*, 391–410. [CrossRef] [PubMed]
10. Wu, C.H.; Liu, I.J.; Lu, R.M.; Wu, H.C. Advancement and applications of peptide phage display technology in biomedical science. *J. Biomed. Sci.* **2016**, *23*, 8. [CrossRef]
11. Gillespie, J.W.; Yang, L.; De Plano, L.M.; Stackhouse, M.A.; Petrenko, V.A. Evolution of a landscape phage library in a mouse xenograft model of human breast cancer. *Viruses* **2019**, *11*, 988. [CrossRef] [PubMed]
12. Han, L.; Liu, P.; Petrenko, V.A.; Liu, A.H. A Label-Free Electrochemical Impedance Cytosensor Based on Specific Peptide-Fused Phage Selected from Landscape Phage Library. *Sci. Rep.* **2016**, *6*, 10. [CrossRef]
13. Han, L.; Wang, D.; Yan, L.; Petrenko, V.A.; Liu, A. Specific phages-based electrochemical impedimetric immunosensors for label-free and ultrasensitive detection of dual prostate-specific antigens. *Sens. Actuators B Chem.* **2019**, *297*, 126727. [CrossRef]
14. Rizzo, M.G.; Carnazza, S.; De Plano, L.M.; Franco, D.; Nicolò, M.S.; Zammuto, V.; Petralia, S.; Calabrese, G.; Gugliandolo, C.; Conoci, S.; et al. Rapid detection of bacterial pathogens in blood through engineered phages-beads and integrated Real-Time PCR into MicroChip. *Sens. Actuators B Chem.* **2021**, *329*, 129227. [CrossRef]
15. Yoo, S.Y.; Merzlyak, A.; Lee, S.W. Synthetic phage for tissue regeneration. *Mediat. Inflamm.* **2014**, *2014*, 192790. [CrossRef]
16. Bazan, J.; Całkosiński, I.; Gamian, A. Phage display-a powerful technique for immunotherapy: 1. Introduction and potential of therapeutic applications. *Hum. Vaccines Immunother.* **2012**, *8*, 1817–1828. [CrossRef] [PubMed]
17. Petrenko, V.A.; Gillespie, J.W.; Xu, H.; O'Dell, T.; De Plano, L.M. Combinatorial avidity selection of mosaic landscape phages targeted at breast cancer cells-an alternative mechanism of directed molecular evolution. *Viruses* **2019**, *11*, 785. [CrossRef] [PubMed]
18. Hartman, E.C.; Jakobson, C.M.; Favor, A.H.; Lobba, M.J.; Álvarez-Benedicto, E.; Francis, M.B.; Tullman-Ercek, D. Quantitative characterization of all single amino acid variants of a viral capsid-based drug delivery vehicle. *Nat. Commun.* **2018**, *9*, 1385. [CrossRef] [PubMed]
19. Han, L.; Shi, J.; Liu, A. Novel biotemplated MnO$_2$ 1D nanozyme with controllable peroxidase-like activity and unique catalytic mechanism and its application for glucose sensing. *Sens. Actuators B Chem.* **2017**, *252*, 919–926. [CrossRef]
20. De Plano, L.M.; Scibilia, S.; Rizzo, M.G.; Crea, S.; Franco, D.; Mezzasalma, A.M.; Guglielmino, S.P.P. One-step production of phage–silicon nanoparticles by PLAL as fluorescent nanoprobes for cell identification. *Appl. Phys. A* **2018**, *124*, 222. [CrossRef]
21. Torrisi, L.; Guglielmino, S.; Silipigni, L.; de Plano, L.M.; Kovacik, L.; Lavrentiev, V.; Torrisi, A.; Fazio, M.; Fazio, B.; di Marco, G. Study of gold nanoparticle transport by M13 phages towards disease tissues as targeting procedure for radiotherapy applications. *Gold Bull.* **2019**, *52*, 135–144. [CrossRef]
22. Henry, K.A.; Arbabi-Ghahroudi, M.; Scott, J.K. Beyond phage display: Non-traditional applications of the filamentous bacteriophage as a vaccine carrier, therapeutic biologic, and bioconjugation scaffold. *Front. Microbiol.* **2015**, *6*, 755. [CrossRef] [PubMed]
23. Mateu, M.G. Virus engineering: Functionalization and stabilization. *Protein Eng. Des. Sel.* **2011**, *24*, 53–63. [CrossRef]
24. Howorka, S. Molecular assembly in natural and engineered systems. *Prog. Mol. Biol. Transl. Sci.* **2011**, *103*, 414.
25. Berchtikou, A.; Sokullu, E.; Nahar, S.; Tijssen, P.; Gauthier, M.A.; Ozaki, T. Comparative study on the inactivation of MS2 and M13 bacteriophages using energetic femtosecond lasers. *J. Biophotonics* **2020**, *13*, e202000109. [CrossRef]
26. De Plano, L.M.; Franco, D.; Rizzo, M.G.; Zammuto, V.; Gugliandolo, C.; Silipigni, L.; Torrisi, L.; Guglielmino, S.P.P. Role of Phage Capsid in the Resistance to UV-C Radiations. *Int. J. Mol. Sci.* **2021**, *22*, 3408. [CrossRef] [PubMed]
27. Morag, O.; Sgourakis, N.G.; Baker, D.; Goldbourt, A. The NMR-Rosetta capsid model of M13 bacteriophage reveals a quadrupled hydrophobic packing epitope. *Proc. Natl. Acad. Sci. USA* **2015**, *112*, 971–976. [CrossRef] [PubMed]
28. Krumova, K.; Cosa, G. Overview of reactive oxygen species. In *Singlet Oxygen: Applications in Biosciences and Nanosciences*; The Royal Society of Chemistry: London, UK, 2016; Chapter 1; Volume 1, pp. 1–21.
29. Lomax, M.E.; Folkes, L.K.; O'Neill, P. Biological consequences of radiation-induced DNA damage: Relevance to radiotherapy. *Clin. Oncol.* **2013**, *25*, 578–585. [CrossRef]
30. Zammuto, V.; Fuchs, F.M.; Fiebrandt, M.; Stapelmann, K.; Ulrich, N.J.; Maugeri, T.L.; Pukall, R.; Gugliandolo, C.; Moeller, R. Comparing spore resistance of Bacillus strains isolated from hydrothermal vents and spacecraft assembly facilities to environmental stressors and decontamination treatments. *Astrobiology* **2018**, *18*, 1425–1434. [CrossRef]
31. Felici, F.; Castagnoli, L.; Musacchio, A.; Jappelli, R.; Cesareni, G. Selection of antibody ligands from a large library of oligopeptides express on a multivalente exposition vector. *J. Mol. Biol.* **2019**, *222*, 301–310. [CrossRef]
32. Luzzago, A.; Felici, F. Construction of disulfide-constrained random peptide libraries displayed on phage coat protein VIII. *Methods Mol. Biol.* **1998**, *87*, 155–164.
33. Carnazza, S.; Foti, C.; Gioffrè, G.; Felici, F.; Guglielmino, S.P.P. Specific and selective probes for *Pseudomonas aeruginosa* from phage-displayed random peptide libraries. *Biosens. Bioelectron.* **2008**, *23*, 1137–1144. [CrossRef]

34. De Plano, L.M.; Carnazza, S.; Franco, D.; Rizzo, M.G.; Conoci, S.; Petralia, S.; Nicoletti, A.; Zappia, M.; Campolo, M.; Esposito, E.; et al. Innovative IgG biomarkers based on phage display microbial amyloid mimotope for state and stage diagnosis in Alzheimer's disease. *ACS Chem. Neurosci.* **2020**, *11*, 1013–1026. [CrossRef]

35. Kay, B.; Winter, J.; McCafferty, J. *Phage Display of Poplides and Proteins: A Laboratory Manual*; Academic Press: San Diego, CA, USA, 1996.

36. Torrisi, L.; Havranek, V.; Cutroneo, M.; Torrisi, A. Gafchromic HD-V2 investigations using MeV ion beams in vacuum. *Radiat. Eff. Defects Solids* **2019**, *174*, 1063–1075. [CrossRef]

37. Nuclear Physics Institute CAS, Rez, Czech Republic. 2021. Available online: http://www.ujf.cas.cz/en/research-development/large-research-infrastructures-and-centres/canam/about-the-project/ (accessed on 15 November 2021).

38. Cutroneo, M.; Havranek, V.; Torrisi, A.; Mackova, A.; Malinsky, P.; Slepicka, P.; Sofer, Z.; Torrisi, L. Polydimethylsiloxane–graphene oxide composite improving performance by ion beam irradiation. *Surf. Interface Anal.* **2020**, *52*, 1156–1162. [CrossRef]

39. Torrisi, L.; Silipigni, L.; Manno, D.; Serra, A.; Nassisi, V.; Cutroneo, M.; Torrisi, A. Investigations on graphene oxide for ion beam dosimetry applications. *Vacuum* **2020**, *178*, 109451. [CrossRef]

40. Ziegler, J.F.; Ziegler, M.D.; Biersack, J.P. SRIM—The stopping and range of ions in matter. *Nucl. Instrum. Methods B* **2010**, *268*, 1818–1823. [CrossRef]

41. Chang, R.L.; Stanley, J.A.; Robinson, M.C.; Sher, J.W.; Li, Z.; Chan, Y.A.; Omdahl, A.R.; Wattiez, R.; Godzik, A.; Matallana-Surget, S. Protein structure, amino acid composition and sequence determine proteome vulnerability to oxidation-induced damage. *EMBO J.* **2020**, *39*, e104523. [CrossRef] [PubMed]

42. Reisz, J.A.; Bansal, N.; Qian, J.; Zhao, W.; Furdui, C.M. Effects of ionizing radiation on biological molecules-mechanisms of damage and emerging methods of detection. *Antioxid. Redox Signal.* **2014**, *21*, 260–292. [CrossRef]

43. Stopar, D.; Spruijt, R.B.; Wolfs, C.J.; Hemminga, M.A. Protein-lipid interactions of bacteriophage M13 major coat protein. *Biochim. Biophys. Acta* **2003**, *1611*, 5–15. [CrossRef]

44. Vos, W.L.; Schor, M.; Nazarov, P.V.; Koehorst, R.B.M.; Spruijt, R.B.; Hemminga, M.A. Structure of membrane-embedded M13 major coat protein is insensitive to hydrophobic stress. *Biophys. J.* **2007**, *93*, 3541–3547. [CrossRef]

45. Hemminga, M.A.; Vos, W.L.; Nazarov, P.V.; Koehorst, R.B.; Wolfs, C.J.; Spruijt, R.B.; Stopar, D. Viruses: Incredible nanomachines. New advances with filamentous phages. *Eur. Biophys. J.* **2010**, *39*, 541–550. [CrossRef] [PubMed]

46. Sommer, R.; Pribil, W.; Appelt, S.; Gehringer, P.; Eschweiler, H.; Leth, H.; Cabaj, A.; Haider, T. Inactivation of bacteriophages in water by means of non-ionizing (UV-253.7 nm) and ionizing (gamma) radiation: A comparative approach. *Water Res.* **2001**, *35*, 3109–3116. [CrossRef]

47. Horneck, G.; Klaus, D.M.; Mancinelli, R.L. Space microbiology. *Microbiol. Mol. Biol. Rev.* **2010**, *74*, 121–156. [CrossRef] [PubMed]